

## THE DUST-SCATTERED X-RAY HALO AROUND *Swift* GRB 050724

S. VAUGHAN<sup>1</sup>, R. WILLINGALE<sup>1</sup>, P. ROMANO<sup>2</sup>, J. P. OSBORNE<sup>1</sup>, M. R. GOAD<sup>1</sup>, A. P. BEARDMORE<sup>1</sup>, D. N. BURROWS<sup>3</sup>, S. CAMPANA<sup>2</sup>, G. CHINCARINI<sup>2,4</sup>, S. COVINO<sup>2</sup>, A. MORETTI<sup>2</sup>, P. T. O'BRIEN<sup>1</sup>, K. L. PAGE<sup>1</sup>, M. A. SUPPER<sup>1</sup>, G. TAGLIAFERRI<sup>2</sup>

Accepted 2005 November 02

### ABSTRACT

This paper discusses the X-ray halo around the *Swift*  $\gamma$ -ray burst GRB 050724 ( $z = 0.258$ ), detected by the *Swift* X-Ray Telescope. The halo, which forms a ring around the fading X-ray source, expands to a radius of  $200''$  within 8 ks of the burst exactly as expected for small-angle X-ray scattering by Galactic dust along the line of sight to a cosmologically distant GRB. The expansion curve and radial profile of the halo constrain the scattering dust to be concentrated at a distance of  $D = 139 \pm 9$  pc (from Earth) in a cloud/sheet of thickness  $\Delta D < 22$  pc. The halo was observed only out to scattering angles of  $200''$ , for which the scattering is dominated by the largest grains, with a maximum size estimated to be  $a_{\max} \approx 0.4 - 0.5 \mu\text{m}$ . The scattering-to-extinction ratio was estimated to be  $\tau_{\text{scat}}/A_V \gtrsim 0.022$ ; this is a lower limit to the true value because contribution from smaller grains, which scatter to larger angles, was not directly observed. The line-of-sight to the GRB passes close to the Ophiuchus molecular cloud complex, which provides a plausible site for the scattering dust.

*Subject headings:* gamma rays: bursts — X-rays: general — Galaxy: structure — ISM:dust

### 1. INTRODUCTION

Small-angle scattering of X-rays by dust grains can produce a ‘halo’ around a distant X-ray source, with a radial intensity distribution that depends on the dust properties and location (Overbeck 1965; Hayakawa 1970; Trümper & Schöfelder 1973). This effect was first detected by Rolf (1983) using *Einsteins* observations of the bright X-ray binary GX 339 – 4, and has subsequently been observed around several other bright Galactic X-ray sources (e.g. Catura 1983; Predehl & Schmitt 1995; Predehl et al. 2000).

Gamma-ray bursts (GRBs) produce high X-ray fluxes for short periods, typically  $\lesssim 1000$  s. Viewed through a substantial column of Galactic dust, these impulsive X-ray events may produce halos that appear to expand on the sky because X-rays scattered at larger angles travel a slightly longer path length to the observer and suffer an increased time delay. This time delay, between the direct and scattered light, means the later observations of the scattered light provide a view of the GRB X-ray emission at earlier times and can, in principle, provide details of the location, spatial distribution and properties of the dust (e.g. Alcock & Hatchett 1978; Klose 1994; Miralda-Escudé 1999; Draine & Bond 2004). In particular, assuming the GRB to lie at a cosmological distance, the distance to the scattering dust can be measured from the radial expansion of the halo, because the halo size increases as  $\theta^2 = 2\tau c/D$ , where  $\tau = t - t_X$  is the time since the pulse of illuminating X-rays and  $D$  is the distance between the dust and observer. Observations of GRB dust haloes can thereby provide very accurate distances to Galactic structures, as first demonstrated by Vaughan et al. (2004) using an *XMM-Newton* observation of the *Integral* GRB 031203.

Electronic address: sav2@star.le.ac.uk

<sup>1</sup> X-Ray and Observational Astronomy Group, University of Leicester, Leicester, LE1 7RH, UK

<sup>2</sup> INAF-Osservatorio Astronomico di Brera, Via Bianchi 46, 23807 Merate, Italy.

<sup>3</sup> Department of Astronomy & Astrophysics, Pennsylvania State University, 525 Davey Lab, University Park, PA 16802, USA.

<sup>4</sup> Università degli studi di Milano-Bicocca, Dipartimento di Fisica, Piazza delle Scienze 3, I-20126 Milan, Italy.

This paper discusses the X-ray halo around GRB 050724, the first halo discovered by *Swift* (Romano et al. 2005) and only the second ever observed around a GRB. The rest of the paper is organised as follows: Section 2 discusses the *Swift* observations and basic data analysis; Section 3 describes the X-ray properties of the burst counterpart during the first few ks of the observation; Section 4 discusses the detailed analysis of the X-ray halo images; Section 5 uses the archival *ROSAT* and *IRAS* data to probe the ISM in the direction of the GRB; and finally the implications of the results of this analysis are discussed in Section 6. Throughout this paper the quoted errors correspond to 90% confidence regions unless stated otherwise.

### 2. OBSERVATIONS AND DATA ANALYSIS

At 2005-07-24 12:34:09 UT the *Swift* Burst Alert Telescope (BAT; Barthelmy 2004) triggered and located GRB 050724 (Covino et al. 2005). The prompt BAT light curve showed a relatively short-lived spike, with a FWHM of  $\approx 0.25$  s (Covino et al. 2005; Krimm et al. 2005), plus an extended low-flux tail lasting for at least  $\gtrsim 200$  s. As discussed by Barthelmy et al. (2005), this burst would have been classified a short burst if observed by BATSE. The total fluence was  $\approx 6.3 \pm 1.0 \times 10^{-7}$  erg cm $^{-2}$  (Krimm et al. 2005) over the 15 – 350 keV band. The spectrum evolves from relatively hard during the 1 s peak (photon index of  $\Gamma = 1.71 \pm 0.16$ ) to much softer ( $\Gamma = 2.5 \pm 0.2$ ) at 50 – 150 s after the trigger.

The spacecraft slewed immediately to the BAT on-board calculated position; the *Swift* X-ray telescope (XRT; Burrows et al. 2004, 2005a) began observations at 12:35:22.9 UT (in automatic state), only 74 s after the BAT trigger, and detected a rapidly fading, uncatalogued X-ray source at (J2000) RA=16<sup>h</sup>24<sup>m</sup>44.4<sup>s</sup>, Dec=  $-27^\circ 32' 28''$  (with a 90% confidence radius of  $6''$ ; Barthelmy et al. 2005). This position is close to the Galactic plane ( $l = 350.37^\circ$ ,  $b = +15.10^\circ$ ); the expected column density of neutral Galactic gas along this line-of-sight (LoS) is  $N_{\text{H}} = 1.46 \times 10^{21}$  cm $^{-2}$  (as measured from 21 cm maps; Dickey & Lockman 1990), and the reddening  $E(B - V) = 0.59$  (from the IR dust maps of Schlegel, Finkbeiner & Davis 1998).

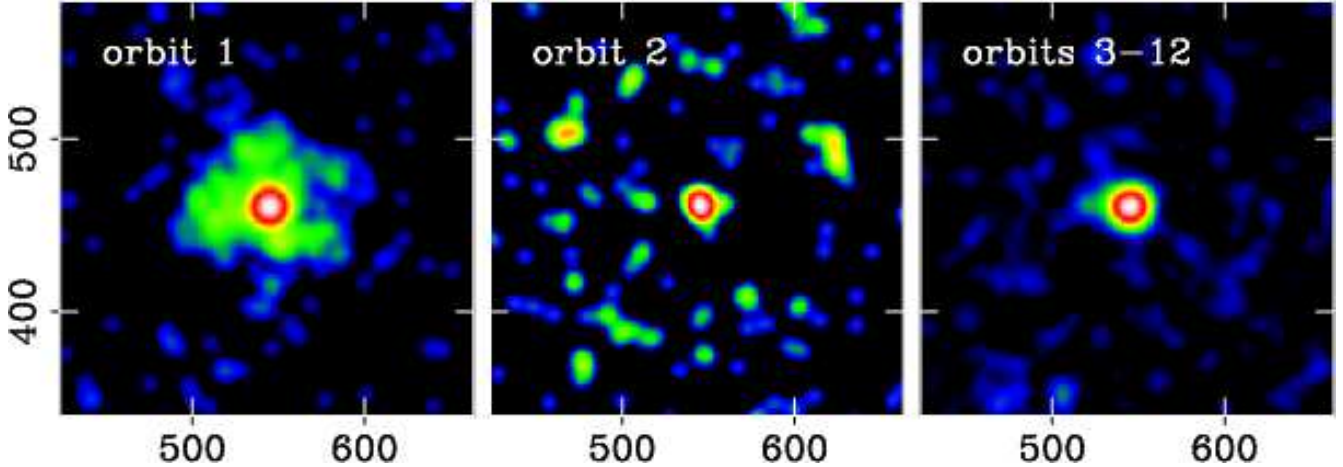


FIG. 1.— 0.2 – 5 keV XRT images of GRB 050724 taken in three time intervals covering the first orbit (343 – 2243 s after  $T_0$ ), second orbit (6068 – 8127 s after  $T_0$ ) and later orbits of *Swift*, plotted in detector coordinates. The images were smoothed using a Gaussian of width 5 pixels ( $\sigma$ ). The X-ray counterpart of GRB 050724 is in the centre of each frame. During orbit 1 the halo expands from a radius of 20 to 44 pixels, during orbit 2 it is visible as a faint ring with a radius of  $\sim 85$  pixels, and in later orbits the halo is not detected.

Follow-up observations revealed a variable optical and radio source within the XRT error circle (4.3 " from the XRT position; Gal-Yam et al. 2005; Soderberg et al. 2005). A 50 ks *Chandra* observation further refined the position of the fading X-ray source and showed it to be coincident with the optical and radio transient (Burrows et al. 2005b). Prochaska et al. (2005) identified the host galaxy of the transient to be a massive early-type galaxy at a redshift of  $z = 0.258 \pm 0.002$  (from Ca H+K and G-band absorption). See also Berger et al. (2005) for a discussion of the host galaxy optical spectrum.

The XRT collected data in Windowed-Timing (WT) mode from 79 – 342 s post-burst (WT mode allows imaging in one spatial dimension only), after which time the data were taken in Photon Counting (PC) mode. WT mode allows imaging in one spatial dimension only, whereas PC mode produces two-dimensional images, see Hill et al. (2004) for a full description of the XRT operating modes. The XRT data were processed by the *Swift* Data Center at NASA/Goddard Space Flight Center (GSFC) to level 1 data products (calibrated, quality flagged event lists). These were further processed with `xrtpipeline v0.8.8` into level 2 data products. In the subsequent analysis only event grades 0 – 2 were used for the WT mode data and only grades 0 – 12 were used for the PC mode data.

### 3. EARLY X-RAY EMISSION FROM GRB 050724

Spectra and light curves were extracted from the WT data using a 40 pixel (94") wide box to define the source and background regions. For the PC mode data, source counts were accumulated from within a circle of radius 25 pixels (59"), and background data were accumulated within an annulus having inner and outer radii of 60 and 100 pixels (141 – 236"). The appropriate ancillary response matrices were generated using `xrtmkarf v0.4.14`.

The spectrum of the WT data (79 – 342 s post-burst) was binned such that each spectral bin contained at least 20 counts and fitted over the 0.6 – 10 keV range<sup>5</sup> using XSPEC (Arnaud 1996). The spectral model comprised a power law continuum modified by two neutral absorbers (modelled using the

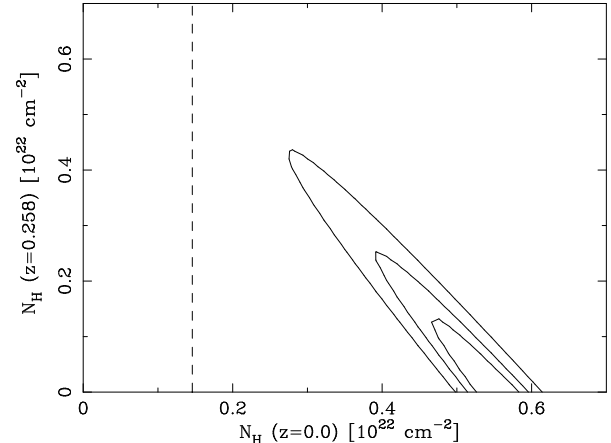


FIG. 2.—  $\Delta\chi^2$  contours for absorption in the host Galaxy ( $z = 0.258$ ) against Galactic absorption ( $z = 0.0$ ). The contours correspond to  $\Delta\chi^2 = 2.30, 4.61$  and  $9.21$ , respectively. The dotted line indicates the expected  $N_H$  based on the 21 cm measurements of Dickey & Lockman (1990).

TBabs code of Wilms, Allen & McCray 2000), one at  $z = 0.0$  and the other at  $z = 0.258$ , corresponding to neutral interstellar gas in our Galaxy and intrinsic to the GRB host galaxy, respectively. Allowing both column densities to be free parameters, this simple model gave a very good fit ( $\chi^2 = 355.89$  for 334 degrees of freedom, dof) with best-fitting parameters as follows:  $\Gamma = 1.94 \pm 0.05$ ,  $N_H(z = 0.0) = 5.9^{+0.3}_{-1.5} \times 10^{21} \text{ cm}^{-2}$  and  $N_H(z = 0.258) < 2.4 \times 10^{21} \text{ cm}^{-2}$ . The Galactic column density inferred from the X-ray spectrum exceeds that expected based on the 21 cm measurements (see Section 2), by  $4.4^{+0.3}_{-1.5} \times 10^{21} \text{ cm}^{-2}$ , and yet there is no clear excess absorption intrinsic to the host galaxy. Figure 2 shows the  $\Delta\chi^2$  contours for the two absorption column densities.

### 4. X-RAY HALO ANALYSIS

#### 4.1. Expansion curve

Figure 1 shows the XRT (PC mode) images from the first, second and later orbits of *Swift*, over the 0.2 – 5 keV en-

<sup>5</sup> The bandpass for the WT-mode spectral fit was restricted to energies above 0.6 keV to avoid calibration uncertainties at lower energies.

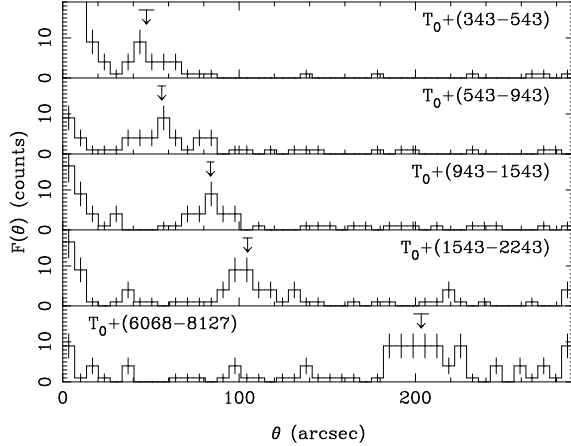


FIG. 3.— Radial profile of counts about the GRB 050724 afterglow from five time intervals. The times are marked in each frame. The arrows mark the maximum likelihood estimate of the halo radius,  $\theta$ , derived from fitting these profiles, and the horizontal bar indicates the 68.3% (1 $\sigma$ ) confidence interval on the radius.

ergy range (only events with energies  $0.2 - 5$  keV were used since the halo has a soft spectrum, as discussed in Section 4.3, and was not detected above 5 keV). The first orbit showed extended emission around the point-like GRB which was dispersed in the second orbit and was difficult to detect in later orbits. In order to better quantify this extension, images were accumulated in five non-overlapping time intervals:  $343 - 543$ ,  $543 - 943$ ,  $943 - 1543$  and  $1543 - 2243$  s from the first orbit and  $6068 - 8127$  s from the second orbit.

Radial profiles were calculated for each image by accumulating the counts in annuli centred on the GRB (see Figure 3). The expanding halo was revealed by the small but significant localised excess of counts, beyond the unresolved GRB<sup>6</sup>. The radius of the halo as a function of time,  $\theta(t)$ , was estimated by fitting each radial profile (using XSPEC) with a model comprising the PSF of the source (a King profile with parameters taken from ground based calibration data; Moretti et al. 2004, 2005) plus a constant background level (per pixel), integrated over the annular bin. A Gaussian was added to represent the profile of the halo, fixing the width to be equal to 10% of the radius:  $\sigma_\theta = 0.1\theta$  (see Section 4.2). The  $C$ -statistic was used to find the maximum likelihood model parameters, appropriate for the case of few counts per bin ( $C = -2 \log \mathcal{L}$ , where  $\mathcal{L}$  is the likelihood; Cash 1979). For each profile, the  $C$ -statistic was minimised and the maximum likelihood position of the Gaussian was used as the radius of the halo in that image. The 90% confidence region for the radius was estimated using the  $\Delta C$  values (see Figure 4).

Figure 5 shows the radius of the halo in each of the five time bins, as measured using the radial profiles. These data were fitted with the function  $\theta(t) = N(t - t_X)^{1/2}$ , which describes the radial expansion of a dust-scattered halo following a (short) X-ray pulse at time  $t_X$  (e.g. Trümper & Schöfeler 1973; Klose 1994; Miralda-Escudé 1999; Draine & Bond 2004). Strictly speaking, this assumes a very narrow pulse of X-rays and an intrinsically narrow dust scattering screen. The value of  $t_X$  corresponds to the typical arrival

<sup>6</sup> The Point Spread Function (PSF) of the XRT has a half-energy radius of  $\approx 8.8''$ , or FWHM  $\approx 9.6''$  at  $E \approx 1.5$  keV (Moretti et al. 2005; Burrows et al. 2004)

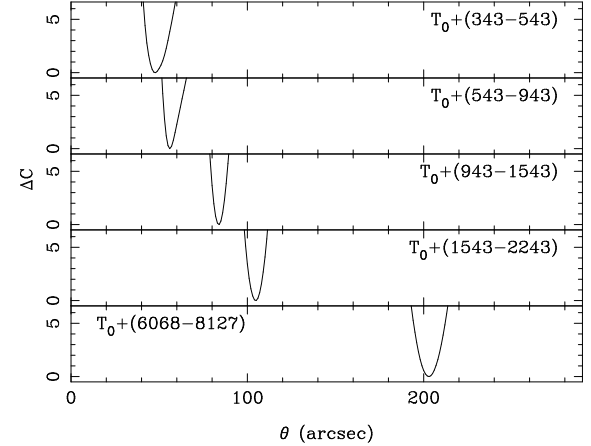


FIG. 4.— Change in  $C$ -statistic as a function of halo position. The minimum of each curve represents the maximum likelihood estimate of the halo radius. Nominal 68.3 and 90% confidence regions can be defined by the intervals bounded by  $\Delta C = 1.0$  and 2.706, respectively.

time of direct (un-scattered) photons, which will be after  $T_0$  since the GRB 050724 remained X-ray bright from  $T_0$  until  $\approx T_0 + 300$  s, meaning almost all the direct X-rays actually arrived after  $T_0$ . The best-fitting values of the free parameters were:  $N = 2.46 \pm 0.08$  (with  $\theta$  measured in arcsec) and  $t_X = 145^{+65}_{-74}$  s after  $T_0$ . This model gave a good fit, with  $\chi^2 = 6.70$  for 4 dof. In order to check whether the best-fitting value of  $t_X$  is plausible, the mean arrival time for the direct X-rays was estimated using the X-ray light curve from the joint BAT-XRT data (Figure 3 of Barthelmy et al. 2005): the flux-weighted photon arrival time<sup>7</sup> over this light curve was  $T_0 + 86$  s, consistent with the best-fitting  $t_X$  from the radial expansion curve.

The normalisation,  $N$ , describes how fast the halo expands and is uniquely determined by the distance to the dust<sup>8</sup>. Assuming the GRB to be at a cosmological distance  $N = (2c/D)^{1/2}$ . The best-fitting normalisation predicts a distance to the scattering medium of  $D = 139 \pm 9$  pc, where the 90% confidence region was calculated with  $t_X$  as a free parameter<sup>9</sup>

This distance measurement is quite robust to the choice of function used to parameterise the halo radial profile. This was demonstrated by repeating the radial profile fitting using different functions to model the halo profile. For each one the halo expansion curve was measured and the distance calculated from its best-fitting normalisation. A Gaussian of fixed width ( $\sigma = 5''$ ) gave  $D = 145 \pm 8$  pc, a Lorentzian of fixed width ( $\Gamma = 10''$ ) gave  $D = 142 \pm 8$  pc and a King model as used to model the PSF (see above) gave  $D = 144 \pm 6$  pc. These different estimates are all well within the confidence region of the original estimate, demonstrating that any systematic errors introduced by the choice of radial profile model are

<sup>7</sup> The flux-weighted photon arrival time was calculated as  $\langle t_X \rangle = \int f_X(t) t dt / \int f_X(t) dt$  where  $f_X(t)$  is the X-ray light curve.

<sup>8</sup> The halo shape is affected by the geometry of the scattering region, and it may not be circular and centred on the GRB image if the scatterer is in the form of a plane-parallel slab not perpendicular to the line-of-sight, or is curved (see Tytenda 2004 for a discussion). However, because of the large ratio of dust distance to halo size, only the most pathological geometries (e.g. slab included at  $> 89^\circ$ ) will produce any observable effect.

<sup>9</sup> This distance estimate is smaller than that given in Romano et al. (2005) because that earlier analysis assumed  $t_X = T_0$ , an assumption not made in the present analysis.

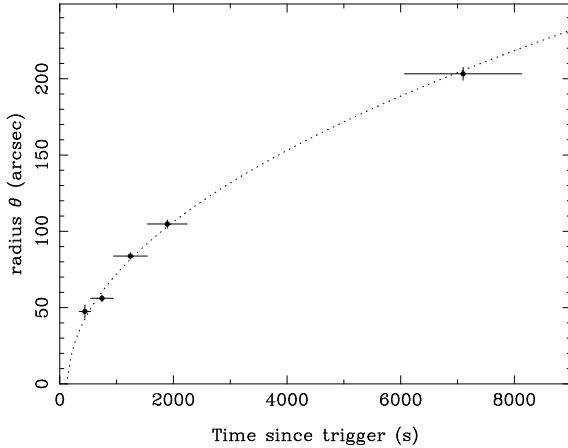


FIG. 5.— Expansion of the ring around GRB 050724 with time. The radii were measured by fitting the local maximum in the radial profiles (Fig. 3). The expansion was fitted with the function  $\theta(t) = N(t - t_0)^{1/2}$  (marked with the dotted line).

smaller than the quoted statistical error.

#### 4.2. Co-moving radial profile

The radial profile of the halo was examined in more detail by summing the five radial profiles (Figure 3), after adjusting the size of the radial bins to correct for the expansion of the halo. A constant background level, estimated from the mean level at large radii, was subtracted from each profile before combining them. The result is shown in Figure 6. This shows that the average radial profile of the halo, after correcting for its expansion, was reasonably narrow. Fitting this profile using a Gaussian to model the halo gave a relative width of  $\text{FWHM}(\theta)/\theta \approx 0.16 - 0.23$  (90% confidence limit).

The observed radial width of the halo is a combination of four terms: (i) the time profile of the illuminating X-ray pulse; (ii) the radial distribution of the dust along the line of sight, (iii) the PSF of the XRT, and (iv) the radial expansion of the halo over the length of an exposure. Term (i) is negligible since the time duration of the initial pulse is short compared to the times (since burst) of the halo images (343 – 8127 s). The XRT PSF (with FWHM of 9.6'') gives rise to a fractional width of 20% in the first image to 5% in the last, meaning term (iii) must contribute significantly to the measured width. The co-moving radial profile is dominated by counts from later images (with longer exposures), during which the fractional increase in the halo radius – term (iv) – was  $\sim 15\%$ . The measured width of the halo may therefore be explained entirely by terms (iii) and (iv), implying the remaining term, the radial thickness of the dust, must be small. A very conservative limit on the physical thickness of the dust cloud along this line of sight is  $\Delta D \approx D \times \text{FWHM}(\theta)/\theta < 22$  pc. Most likely the dust is confined in a much narrower region.

#### 4.3. Halo spectrum

The spectrum of the halo was extracted from the first orbit of data using an annular extraction region with inner and outer radii of 20 and 45 pixels (47 – 106 arcsec), respectively. A background spectrum was extracted from an annulus with radii of 60 and 100 pixels and an appropriate ancillary response file was generated. Due to the small number of counts ( $\approx 100$ ) the spectrum was fitted using the  $C$ -statistic, rather

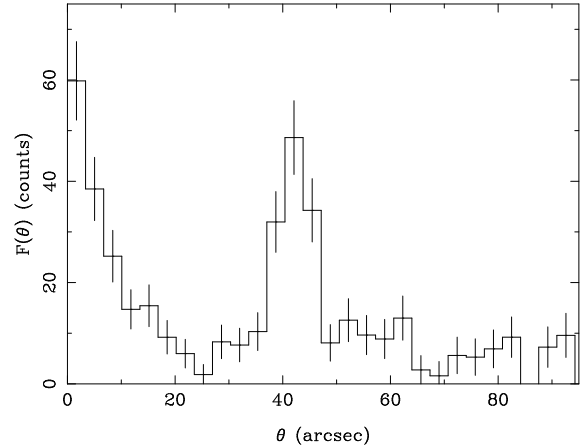


FIG. 6.— Co-moving radial profile around GRB 050724. This shows the counts accumulated in annuli around the GRB summed over the five time intervals of Figure 3, after correcting for the expansion of the halo (matching the radii to those from the first image). The halo occurs at  $\theta \approx 45$  arcsec from the GRB ( $\theta = 0$ ) and is a relatively narrow ( $\sigma_\theta/\theta \approx 0.07$ ) structure.

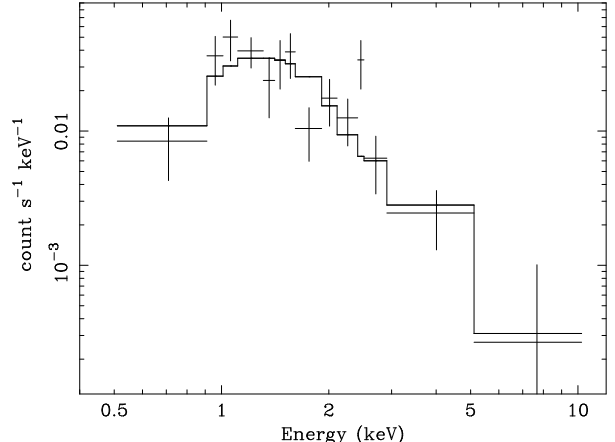


FIG. 7.— XRT spectrum of the halo during the first *Swift* orbit. Crosses mark the data and the histogram marks the best-fitting absorbed power law model. The data were binned for illustration purposes only.

than binning to 20 counts per bin and fitting using the  $\chi^2$  statistic, which would result in very few bins. The spectral model used was an absorbed power law, with the neutral absorption column density fixed at the value obtained from the early XRT spectrum ( $N_H = 5.9 \times 10^{21} \text{ cm}^{-2}$ ; section 3). The data are shown in Figure 7. The best fitting photon index was  $\Gamma = 2.7^{+0.5}_{-0.3}$ , significantly steeper than the GRB X-ray spectrum ( $\Gamma = 1.94 \pm 0.05$ ), as expected due to the strong energy dependence of the dust scattering cross section. The model gave a good fit, with a rejection probability of only  $p = 0.31$  estimated using  $10^3$  Monte Carlo simulations. The mean photon energy in the binned, background subtracted halo spectrum was  $\langle E \rangle = 1.54$  keV.

#### 4.4. Halo flux as a function of angle

The flux decay of the halo was also estimated using the radial profile of the combined image from orbits 1 and 2 (over which the halo is well-detected). Counts were accumulated in annuli of width  $\Delta\theta = 17.6''$  (7.5 pixels) and background subtracted assuming a constant background level per pixel es-

timated from an annulus enclosing  $280 - 370''$ . The sampling of the halo as a function of angle is incomplete, due to the incomplete time coverage of the observation, therefore radii over which the halo was not observed were masked out of the radial profile. The masking was done by converting the times of the observations into radii using the best-fitting expansion curve (Figure 5) and removing all radial bins containing unobserved angles. The result is shown in Figure 8.

The total fluence of scattered light (in the halo),  $F_H$ , should be related to the direct light (i.e. un-scattered light from the GRB),  $F_X$ , by:

$$\frac{F_H}{F_H + F_X} = 1 - e^{-\tau_{\text{scat}}} \quad (1)$$

where  $\tau_{\text{scat}} = \sigma N_g$  is the scattering optical depth, with  $\sigma$  the total scattering cross-section and  $N_g$  is the dust grain column density along the LoS (e.g. equation 14 of Mauche & Gorenstein 1986, henceforth MG86). For low optical depths ( $\tau_{\text{scat}} \ll 1$ ), where multiple scattering is insignificant, this can be approximated by  $F_H \approx \tau_{\text{scat}} F_X$ . The above quantities represent the entire halo (integrated over all scattering angles) but the scattering cross-section is a function of angle which defines the halo fluence per unit angle. In the Rayleigh-Gans approximation<sup>10</sup> the differential scattering cross-section for a spherical grain of size  $a$  (in units of  $\mu\text{m}$ ) is given by:

$$\frac{d\sigma}{d\Omega} = A_E a^6 \left[ \frac{j_1(x)}{x} \right]^2 (1 + \cos^2 \theta) \quad (2)$$

(equation 2.2 of Hayakawa 1970) where  $A_E$  is a normalisation that depends on the energy of X-rays being scattered,  $x = (4\pi a/\lambda) \sin(\theta/2)$  and  $j_1(x) = (\sin x)/x^2 - (\cos x)/x$  is the spherical Bessel function of the first order. The central core of this function is approximately Gaussian, leading to a halo with a characteristic size  $\theta_{\text{rms}} \approx 62.4(aE)^{-1}$  arcsec (equation 6 of MG86; Hayakawa 1970). Using equation 2 the scattered fluence in the halo per unit scattering angle is:

$$\frac{dF_H}{d\theta} = A_E a^6 2\pi \theta \left[ \frac{j_1(x)}{x} \right]^2 (1 + \cos^2 \theta) N_g F_X \propto a^6 \theta \left[ \frac{j_1(x)}{x} \right]^2 (1 + \cos^2 \theta) \quad (3)$$

which peaks at  $\theta \approx \theta_{\text{rms}}$ .

This function was fitted to the data (solid curve in Figure 8) yielding a best-fitting value of  $a = 0.367 \mu\text{m}$  (with a 90% confidence region of  $0.316 - 0.430 \mu\text{m}$ ), assuming a typical energy of  $E \approx 1.54 \text{ keV}$  for the scattered X-rays (see section 4.3). The scattering of soft X-rays is dominated by the largest grains, due to the strong dependence of the scattering cross-section on grain size (the total scattering cross section, integrated over all angles is  $\sigma \propto a^4$ ), and so this estimate for  $a$  corresponds to grains close to the maximum grain size. This best-fitting model was integrated over all angles to estimate the total halo fluence of  $F_H \approx 342 \pm 34$  counts (where the  $1\sigma$  error was approximated by the 10% fractional error on the total observed halo fluence).

The above calculation is valid for a single grain size which should be a reasonable approximation given the strong dependence of the scattering cross-section on  $a$ . The presence

<sup>10</sup> Smith & Dwek (1998) demonstrated that the Rayleigh-Gans theory and the more exact Mie theory are in close agreement for photons energies  $E \approx 2 \text{ keV}$  and typical grain sizes.

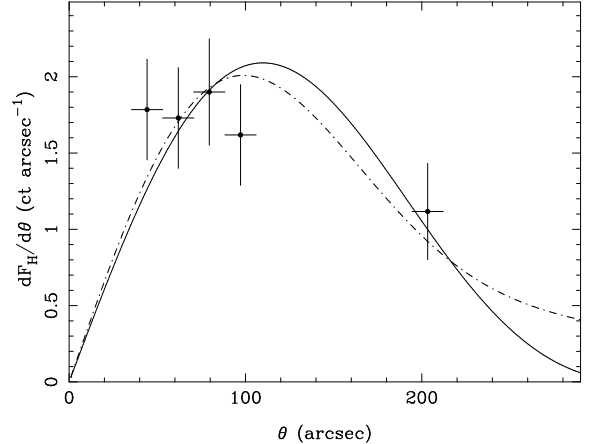


FIG. 8.— Halo flux as a function of scattering angle. The crosses show the background-subtracted counts per (equal size) radial bin over which the halo was detected. The solid curve marks the best-fitting theoretical scattering curve  $dF_H/d\theta$  (Equation 3) assuming a single grain size ( $a = 0.367 \mu\text{m}$ ). The dot-dashed line shows the best-fitting function assuming a MRN distribution of grain sizes (with  $a_{\text{max}} = 0.524 \mu\text{m}$ ).

of smaller grains will however cause the halo fluence to fall off less rapidly at large angles and this extended ‘tail’ could contain substantial additional fluence. In order to investigate the consequence of a continuous grain size distribution, equation 3 was re-calculated at each angle by integrating over the grain size distribution  $N(a)$ . The size distribution was assumed to follow that of Mathis, Rumpl & Nordsieck (1977; hereafter MRN):

$$N(a) = \begin{cases} N_0 a^{-q} & a_{\text{min}} \leq a \leq a_{\text{max}} \\ 0 & \text{elsewhere} \end{cases} \quad (4)$$

The revised function was fitted to the data assuming  $a_{\text{min}} \approx 0.04 \mu\text{m}$  and  $q = 3.5$ , yielding a best-fitting  $a_{\text{max}} = 0.524 \mu\text{m}$  (with a 90% confidence region  $0.426 - 0.790 \mu\text{m}$ ), this is slightly larger than, but not inconsistent with other estimates derived from X-ray haloes (MG86; Predehl et al. 1991; Clark 2004). The best-fitting model is also shown in Figure 8 (dot-dashed curve). The fit is not very sensitive to  $a_{\text{min}}$ <sup>11</sup> as long as  $a_{\text{max}}/a_{\text{min}} \gtrsim 5$  and  $q \gtrsim 3.5$ . The total fluence in this model, integrated over all angles, was virtually identical to the single grain size model ( $\approx 343 \pm 34$  counts), although the fluence could be higher if there is a greater contribution from smaller grains scattering to larger angles that were not directly observed.

#### 4.5. Scattering optical depth

Given the above estimate of the halo fluence,  $F_H$ , it is possible to estimate the dust scattering optical depth once the direct GRB X-ray fluence,  $F_X$ , is known. This latter quantity can be estimated by integrating the combined XRT-BAT light curve of the burst. Figure 3 of Barthelmy et al. (2005) shows the X-ray light curve of GRB 050724 from  $T_0$ . This was produced using the XRT observations after  $T_0 + 79$  s, and the  $15 - 25 \text{ keV}$  BAT light curve extrapolated into the XRT band based on a spectral fit to the simultaneous BAT and XRT spectrum. During the first  $\sim 300$  s after the trigger the

<sup>11</sup> Using  $a_{\text{min}} = 0.004 \mu\text{m}$  or  $0.1 \mu\text{m}$  changed the fit statistic by only  $\Delta\chi^2 = +0.009$  or  $+0.038$ , respectively.

X-ray source was bright; the WT data contain  $\sim 1.18 \times 10^4$  source counts (0.2–10 keV). The extrapolated BAT data predict almost exactly the same number of counts prior to the start of the XRT/WT observation. Although there will be a systematic error associated with the extrapolation of the BAT data to lower energies, the tight agreement between BAT and XRT data in the interval of overlap suggests this is likely to be small (Barthelmy et al. 2005). Together these give a total of  $\approx 2.42 \times 10^4$  counts. Combining this with the  $F_H$  value of section 4.4 gave  $\tau_{\text{scat}} \approx F_H/F_X \approx 0.014$ . Making an approximate correction to an effective scattering optical depth at 1 keV gives  $\tau_{\text{scat}}(1 \text{ keV}) \approx \tau_{\text{scat}}(E)E^2 = 0.034$  (with  $E$  the mean scattered photon energy in keV).

### 5. ISM TOWARDS GRB 050724

Archival *ROSAT* and *IRAS* data were used to constrain the ISM in the direction of GRB 050724. The top two panels of Figure 9 show the soft X-ray sky around GRB 050724, derived from the *ROSAT* All-Sky Survey (RASS) data in the 0.4–1.2 keV band, and the bottom panel shows the *IRAS* All-Sky Survey 100  $\mu\text{m}$  map of the region. These images reveal structures dominated by the Ophiuchus molecular cloud complex casting the dark ‘shadows’ in the *ROSAT* map (middle panel) and enhanced IR dust emission in the *IRAS* map (lower panel). The main  $\rho$  Oph molecular cloud (L1688; Klose 1986) is the in the bright region in the upper-left part of the *IRAS* map. These data were used to estimate the column density in the cloud by comparing the column density estimates for the GRB position to those at locations ‘A’ and ‘B,’ chosen to be representative of nearby but off-cloud lines-of-sight.

The column densities were estimated in three independent ways, and the results are presented in Table 1. The first estimates comes from the Dickey & Lockman (1990) 21 cm maps of  $N_H$ . This shows little change in  $N_H$  between the three positions (see Table 1), and this was confirmed by the 21 cm map of the region shown by de Geus & Burton (1991; see their figure 5). The column density due to the intervening cloud in the direction of GRB 050724 was estimated from the difference between the column density towards the GRB and the mean of that measured for A and B. This gave  $N_H = 0.05 \pm 0.20 \times 10^{21} \text{ cm}^{-2}$  (where the uncertainty is a very rough estimate based on half the difference between A and B). In other words there is no excess H I in the direction of GRB 050724 due to the intervening dust cloud.

The second estimate comes from the IR reddening maps from Schlegel et al. (1998). This gave  $E(B - V)$  values, based on the *COBE* temperature and *IRAS* intensity at the position of interest, of 0.59, 0.17 and 0.25 for the GRB, A and B, respectively. These correspond to optical extinctions of  $A_V = 2.37, 0.68$  and  $1.01$ , respectively, assuming  $R_V \equiv A_V/E(B - V) = 4.0$  as measured by Vrba, Coyne & Tapia (1993) in the direction of the  $\rho$  Oph cloud. The reddening values were converted to hydrogen column densities assuming  $N_H = 4.93 \times 10^{21} E(B - V) \text{ cm}^{-2}$  (Diplas & Savage 1994). In this case the excess column density over the GRB was  $N_H = 1.9 \pm 0.2 \times 10^{21} \text{ cm}^{-2}$ . However, as noted by Jura (1980), Vuong et al. (2003) and others, the dust-to-gas conversion factors in the direction of the Oph cloud are uncertain due to the complexity of modelling the cloud medium.

The third estimate was derived from RASS spectra extracted<sup>12</sup> using  $0.5^\circ$  radius regions centred on the positions

<sup>12</sup> *ROSAT* count rates in different channels were extracted using the HEASARC “X-ray background tool” available via the following address:

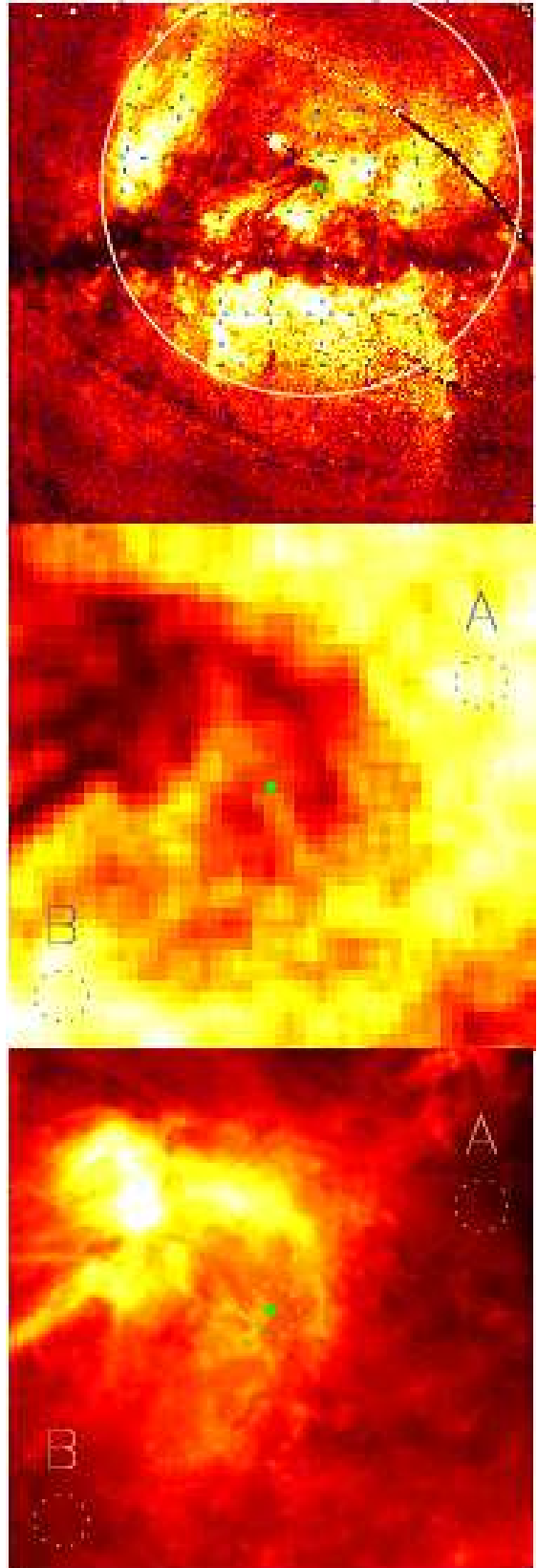


FIG. 9.— X-ray and IR images of the sky around GRB 050724. Upper panel: 0.4–1.2 keV *ROSAT* All-Sky Survey (RASS) map in Galactic coordinates spanning  $102^\circ$  on a side. The position of GRB 050724 is marked with the small filled circle, the large circle marks the extent of the super-bubble centred on the Sco-Cen OB association. Middle panel:  $10^\circ \times 10^\circ$  close up of the RASS map around GRB 050724 (marked with the filled circle). The dotted circle has a radius of  $0.5^\circ$ , which corresponds to  $\approx 2.4 \text{ pc}$  at the distance to the scattering dust. Lower panel: 100  $\mu\text{m}$  *IRAS* map on the same scale as the middle panel. Clearly the IR emission and soft X-ray absorption are well correlated. Again the position of the GRB is indicated by the filled circle. Positions ‘A’ and ‘B’ mark the off-cloud regions discussed in the text.

TABLE 1  
COMPILATION OF GALACTIC COLUMN DENSITY ESTIMATES

Technique	Reference	$N_{\text{H}}$ [GRB] ( $10^{21} \text{ cm}^{-2}$ )	$N_{\text{H}}$ [A] ( $10^{21} \text{ cm}^{-2}$ )	$N_{\text{H}}$ [B] ( $10^{21} \text{ cm}^{-2}$ )
21 cm	1	1.46	1.22	1.61
IR map	2	2.92	0.83	1.24
RASS	3	3.57	0.52	1.28

REFERENCES: (1) Dickey & Lockman (1990), (2) Schlegel et al. (1998), (3) this work

of the GRB, A and B. These were fitted with the model developed by Willingale et al. (2003) but, due to the complexity of the model and low resolution of the data, most parameters were fixed at the values found from an analysis of nearby *XMM-Newton* fields (M. A. Supper, in prep.). The two parameters allowed to vary in the fit were the foreground absorption column density and the emission measure of the “Loop I super-bubble” (indicated by the large circle in the top panel of Figure 9). The excess column density towards GRB 050724 was estimated, by comparison with A and B, at  $N_{\text{H}} = 2.7 \pm 0.4 \times 10^{21} \text{ cm}^{-2}$ . Given the systematic errors involved in modelling the complex X-ray spectrum, and converting from dust reddening factor to equivalent hydrogen column density, the X-ray and IR derived estimates are in reasonable agreement.

## 6. DISCUSSION

The X-ray halo around GRB 050724, as observed by the *Swift* XRT, has provided accurate information on the Galactic dust distribution in this direction. In particular, the narrow halo must be caused by a concentration of dust at a distance of  $D = 139 \pm 9 \text{ pc}$  from Earth, in a cloud or sheet with a thickness  $\Delta D < 22 \text{ pc}$ . The radial profile of the halo constrains the size of the largest grains to be  $a_{\text{max}} \sim 0.4 - 0.5 \mu\text{m}$ , but the contribution from smaller grains is unconstrained because the halo was not detected at scattering angles larger than  $\theta \approx 200''$ . The estimated value of  $a_{\text{max}}$  is higher than the often used value of  $0.25 \mu\text{m}$  (MRN; see also Predahl & Schmitt 1995), although this is not without precedent as Jura (1980) previously noted that the non-standard optical extinction curves in the direction of  $\rho$  Ophiuchus may signify the presence of unusually large grains.

The LoS to GRB 050724 includes the Upper Scorpius subgroup of the Scorpius-Centaurus OB association at a mean distance of  $145 \pm 2 \text{ pc}$  (derived from *HIPPARCOS* data; de Zeeuw et al. 1999). There is considerable structure in the extinction maps around this region, including material belonging to the Ophiuchus molecular cloud complex (de Geus 1992). Knude & Høg (1998) detected a sharp rise in the reddening at  $120 - 150 \text{ pc}$  in the direction of the  $\rho$  Oph star forming region, which is consistent with the distance measured for the dust responsible for the X-ray halo. If the X-ray scattering dust is associated with part of the Oph molecular cloud complex, this gives the most accurate measurements to date for the distance to the cloud and its physical thickness.

The excess optical extinction in the direction of the GRB 050724, compared to the mean of the off-cloud positions

‘A’ and ‘B’, was  $A_V = 1.5 \text{ mag}$  (Section 5). In combination with the estimated halo scattering optical depth (Section 4.5) this gives  $\tau_{\text{scat}}/A_V \approx 0.022$  at 1 keV. This is lower than the value of 0.056 estimated by Predahl & Schmitt (1995) using *ROSAT* observations of bright Galactic X-ray sources, and a factor of a few lower than the value derived from the model of Draine (2003). However, the halo around GRB 050724 was only observed at small angles ( $\theta \lesssim 200''$ ) and so the flux contribution from smaller grains is largely unconstrained, meaning that the true halo flux, and hence  $\tau_{\text{scat}}$ , is probably larger.

As shown by Figure 9, the X-ray absorption and IR dust emission are well-correlated, demonstrating they are caused by the same medium. By contrast the 21 cm map shows little correlation with these images (Figure 5 of de Geus & Burton 1991), suggesting the cloud medium has a comparatively low density of atomic H I. The most obvious explanation is that the hydrogen is molecular, although there is no obvious CO emission from this location in figure 3 of de Geus, Bronfman & Thaddeus (1990). The Ly- $\alpha$  map of the region (see figure 13 of de Geus et al. 1990) shows two nearby H II regions, known as S9 and RCW 129, around the stars  $\sigma$  Sco (B1 III) and  $\tau$  Sco (B0 V), respectively. It is therefore also plausible that some fraction of the atomic hydrogen is ionised by these nearby young stars (with distances of  $\sim 140 \text{ pc}$ ; Shull & van Steenberg 1985). The total Galactic hydrogen column density along the LoS to GRB 050724 is therefore the sum of that revealed by the 21 cm H I maps and that inferred from the molecular cloud (mostly H<sub>2</sub> and/or H II). The 21 cm measurement of the total H I column density gave  $1.5 \times 10^{21} \text{ cm}^{-2}$ , whereas the column density in the dust cloud was measured at  $1.9 \pm 0.2 \times 10^{21} \text{ cm}^{-2}$  from the excess IR emission and  $2.7 \pm 0.4 \times 10^{21} \text{ cm}^{-2}$  from the excess soft X-ray absorption (Section 5). The total hydrogen column density is therefore in the range  $3.4 - 4.2 \times 10^{21} \text{ cm}^{-2}$ , slightly lower than that measured from the GRB X-ray spectrum ( $4.4 - 6.2 \times 10^{21} \text{ cm}^{-2}$ ; Section 3). It is of course possible that this extra X-ray absorption along the LoS to GRB 050724 ( $\Delta N_{\text{H}} \sim 1.5 \times 10^{21} \text{ cm}^{-2}$ ) is caused by either a modest column of molecular or ionised gas on the far side of the Sco-Cen super-bubble, or due to cold gas in the GRB host galaxy, the formal constraint on which was  $N_{\text{H}} < 2.4 \times 10^{21} \text{ cm}^{-2}$  (Section 3).

*Note added in proof:* Since the completion of this paper Tiengo & Mereghetti (2005) have announced the detection of another dust-scattered X-ray halo around a GRB. This brings the total number of known GRB X-ray halos to three.

SV, MRG, KP, APB, JPO and MAS gratefully acknowledge funding through the PPARC, UK. This work is supported at Pennsylvania State University (PSU) by NASA contract NAS5-00136, at the University of Leicester (UL) by the Particle Physics and Astronomy Research Council on grant number PPA/Z/S/2003/00507, and at the Osservatorio Astronomico di Brera (OAB) by funding from ASI on grant number I/R/039/04. We gratefully acknowledge the contributions of dozens of members of the XRT team at PSU, UL, OAB, GSFC, ASI Science Data Center, and our subcontractors, who helped make this instrument possible. We thank an anonymous referee for a thoughtful report.

<http://heasarc.gsfc.nasa.gov/>

## REFERENCES

Alcock C., Hatchett S., 1978, ApJ, 222, 456  
Arnaud K., 1996, in: *Astronomical Data Analysis Software and Systems*, Jacoby G., Barnes J., eds, ASP Conf. Series Vol. 101, p17

Barthelmy S. D., 2004 SPIE 5165, 175  
 Barthelmy S. D., et al. 2005, Nature, in press  
 Berger E., et al. , 2005, Nature, submitted (astro-ph/0508115)  
 Burrows D. N. et al. . 2004, SPIE, 5165, 201  
 Burrows D. N. et al. . 2005a, Sp. Sc. Rev., in press (astro-ph/0508071)  
 Burrows D. N., et al. 2005b, GCN 3697  
 Carrasco L., Strom S. E., Strom K. M., 1973, ApJ, 182, 95  
 Cash W., 1979, ApJ, 288, 939  
 Catura R. C., 1983, ApJ, 275, 645  
 Clark G. W., 2004, ApJ, 610, 956  
 Covino S. et al. 2005, GCN 3665  
 de Geus E. J., Burton W. B., 1991, A&A, 246, 559  
 de Geus E. J., 1992, A&A, 262, 258  
 de Zeeuw P. T., Hoogerwerf R., de Bruijne J. H. J., Brown A. G. A., Blaauw A., 1999; AJ, 117, 354  
 Dickey J.M., Lockman F.J. 1990, ARA&A, 28, 215  
 Diplas A., Savage B. D., 1994, ApJ, 427, 274  
 Draine B.T., 2003, ApJ, 598, 1026  
 Draine B.T., Bond N. A., 2004, ApJ, 617, 987  
 Gal-Yam A., et al. 2005, GCN 3681  
 Gehrels N., et al. 2004, ApJ 611, 1005.  
 Hayakawa S., 1970, Prog. Theor. Phys., 43, 1224  
 Hill J. E. et al. 2004, SPIE, 5165, 217  
 Jura M., 1980, ApJ, 235, 63  
 Klose S. 1986, ApSS, 128, 135  
 Klose S. 1994, A&A, 289, L1  
 Knude J., Høg E., 1998, A&A, 338, 897  
 Krimm H., et al. 2005, GCN 3667  
 Mauche, C.W., Gorenstein, P. 1986, ApJ, 302, 371 (MG86)  
 Mathis J. S., Rumpf W., Nordsieck K. H., 1977, ApJ, 217, 425 (MRN)  
 Miralda-Escudé 1999, ApJ, 512, 21  
 Moretti A., et al. 2004, SPIE, 5165, 232  
 Moretti A., et al. 2005, SPIE, in press  
 Overbeck J.W. 1965, ApJ, 141, 864  
 Predehl, P., Bräuniger, Burkert, W., Schmitt, J.H.M.M. 1991, A&A, 246, L40  
 Predehl P., Schmitt J.H.M.M. 1995, A&A, 293, 889  
 Predehl P., Burwitz V., Paerels F., Trümper, J., 2000, A&A, 357, L25  
 Prochaska J. X., et al. 2005, GCN 3700  
 Rolf D.P. 1983, Nature, 302, 46  
 Romano P., et al. 2005, GCN 3685  
 Schlegel D. J., Finkbeiner D. P., Davis M., 1998, ApJ, 500, 525  
 Shull J. M., van Steenberg M. E., 1985, ApJ, 294, 599  
 Smith R. K., Dwek E., 1998, ApJ, 503, 831  
 Soderberg A. M., Cameron P. B., Frail D. A., 2005, GCN 3684  
 Tiengo A., Mereghetti S., 2005, A&A, in press (astro-ph/0511186)  
 Trümper J., Schönfelder V. 1973, A&A, 25 445  
 Tylenda R., 2004, A&A, 414, 223  
 Vaughan S. et al. 2004, ApJ, 603, L5  
 Vrba F., Coyne G., Tapia S., 1993, AJ, 105, 1010  
 Vuong M. H., Montmerle T., Grossi N., Feigelson E. D., Verstraete L., Ozawa H., 2003, A&A, 408, 581  
 Watson D., et al. 2005, ApJ, submitted  
 Willingale R., Hands A. D. P., Warwick R. S., Snowden S. L., Burrows D. N., MNRAS 343, 995, 2003  
 Wilms J., Allen A., McCray R., 2000, ApJ, 542, 914